Line filtering for detection of microtools in 3D ultrasound data

Marián Uherčík*†, Jan Kybic*, Christian Cachard† and Hervé Liebgott†

*Center for Machine Perception, Department of Cybernetics, Faculty of Electrical Engineering,
Czech Technical University, Prague, Czech Republic
†CREATIS-LRMN, Universite de Lyon, INSA-Lyon, Universite Lyon 1, CNRS UMR 5220, Inserm U630,
Villeurbanne, France

***Abstract*—We propose a robust method for localization of elongated surgical tools in 3D ultrasound data based on shape analysis. The tubular structures in input data are enhanced by a line filter in the pre-processing phase. A new model of a surgical tool appearance in 3D ultrasound image is proposed which exploits its tubular shape. The tool axis is estimated with robust model fitting using a randomized RANSAC procedure. The tool model requires the voxels close to the axis to have a high intensity, high tubularness, and the local principal directions to be consistent with the tool axis.**

The visual contrast of the tool can be enhanced four-fold using line filtering. We demonstrate that classification rate is improved by 25-40% when adding the tubularness attribute. The comparison to other state-of-the-art localization methods shows that the proposed method is the most robust for data with high level of noise at the expense of additional time for pre-processing (less than 10 seconds for volume of size 53×71×260 voxels).

I. Introduction

Minimally invasive surgical procedures (such as needle biopsy [1] or electrode insertion [2]) involve an insertion of a thin tubular microtool of diameter $1\ \mathrm{mm}$ and less. Precise navigation of such surgical instruments is essential for reducing the damage of tissue caused by failed insertions. When medical imaging techniques (e.g. MRI, CT) are combined with stereotactic frame, a sub-milimeter accuracy can be achieved [3]. Ultrasound (US) monitoring of the tool insertion is clinically used because there is no-ionizing radiation, it provides images at real-time speed and has relatively low costs.

The observation of such a microtool in US image is a difficult task. The lateral resolution of the ultrasound is approximately the same as the diameter of tool. There is a strong speckle noise and other acoustic artifacts which make the appearance of a metallic tool irregular. The doctors are trained for visual localization of tools in 2D US images. Our first aim is to enhance the appearance of the tool to aid visual localization. Second, we want to apply the new shape related description to improve our previously published automatic localization method. The output of this method can be used for visualization, to select the 2D slice containing the tool.

A. Previous work

Variety of algorithms for object localization in ultrasound data has been proposed. Barva et. al [4] uses the Parallel Integral Projection (PIP) to localize a straight cylindrical objects in 3D images. This approach is based on the observation that projection area of a tool is minimized when the projection is performed along the tool axis. Multi-resolution PIP and early stopping can be used for speed-up [5].

The Hough Transform (HT) [6] is widely used for a straight line detection in 2D images but it can be generalized to 3D. Ding et al. use a more efficient Randomized HT (RHT) [7] for straight needle segmentation in thresholded 3D ultrasound images. Quick RHT (QRHT) [8] reduces the computational effort by doing RHT only in coarse resolution volumes and subsequently refining the solution.

Uherčík et al. [9] use a model fitting using RANSAC for tool localization in 3D US. The axis is modelled as a polynomial curve (or a straight line) in thresholded data. The location of the tool axis is estimated by the RANSAC [10] and refined by local optimization. This approach is robust to background noise and fast enough for a real-time application. In this work, we further increase its robustness by applying a shape based tool model using line filtering (Section II-B).

B. Line filtering

Previous methods assume the tool to appear as a high intensity cylinder in US data. We can use an additional assumption that the tool is a one-dimensional (1D) straight structure to distinguish it better from background structures which are 2D (e.g. layers of fat tissue).

The idea of line filtering comes from vessel enhancement e.g. in MR angiography [11]. The cylindrical tool in US images can be enhanced using the same methods (Section II-A).

II. Method

The proposed method consists of two phases: a) pre-processing by line filtering (Section II-A) for enhancement of the tubular structures which likely belong to the tool, b) tool localization by model fitting using the RANSAC procedure (Section II-B).

A. Line filtering

The line filtering pre-computes two attributes for each voxel $\mathbf{x} \in \mathcal{X}$: tubularness $J(\mathbf{x})$ and local principal direction $\mathbf{k}(\mathbf{x})$.

Intensity variations are analyzed via second order derivatives. The image function is approximated using a Taylor expansion in the proximity of a point $\mathbf{x}$:

$$I(\mathbf{x}+\mathbf{d}) \approx I(\mathbf{x}) + \mathbf{d}^{\mathrm{T}} \nabla I(\mathbf{x}) + \frac{1}{2}\mathbf{d}^{\mathrm{T}}\mathbf{H}(\mathbf{x})\mathbf{d}, \qquad (1)$$

where $\mathbf{d}$ is a perturbation vector. The gradient vector $\nabla I(\mathbf{x})$ and the Hessian matrix

$$\mathbf{H}(\mathbf{x}) = \begin{bmatrix} I_{xx}(\mathbf{x}) & I_{xy}(\mathbf{x}) & I_{xz}(\mathbf{x}) \\ I_{yx}(\mathbf{x}) & I_{yy}(\mathbf{x}) & I_{yz}(\mathbf{x}) \\ I_{zx}(\mathbf{x}) & I_{zy}(\mathbf{x}) & I_{zz}(\mathbf{x}) \end{bmatrix} \qquad (2)$$

are computed by the convolution of the image function I with the derivatives of the symmetrical Gaussian [12]

$$I_{\alpha\beta}(\mathbf{x}) = I(\mathbf{x}) * \frac{\partial^2}{\partial\alpha\partial\beta} G(\mathbf{x}, s). \qquad (3)$$

The scale s of Gaussian $G(\mathbf{x}, s)$ corresponds to the apparent radius of the tool and can be learned from a training set of images with ground-truth.

The eigenanalysis of the Hessian matrix $\mathbf{H}(\mathbf{x})$ characterizes the second order local structure of voxels centered at the tube. Let $|\lambda_1| \leq |\lambda_2| \leq |\lambda_3|$ be its eigenvalues and $\mathbf{e}_1$, $\mathbf{e}_2$, $\mathbf{e}_3$ corresponding eigenvectors. For voxels in tubular structure, one eigenvalue λ_1 is small and the other two λ_2, λ_3 big:

$$(0 \approx |\lambda_1|) \text{ and } (|\lambda_1| \ll |\lambda_2|) \text{ and } (\lambda_2 \approx \lambda_3) \qquad (4)$$

The local principal direction is returned

$$\mathbf{k}(\mathbf{x}) = \mathbf{e}_1 / \|\mathbf{e}_1\|. \qquad (5)$$

Various *tubularness* measures $J(\mathbf{x})$ have been proposed for tool enhancement in 3D image (Fig. 1). We assume a bright cylinder on dark background, so the voxels with $\lambda_3 \geq 0$ or $\lambda_2 \geq 0$ can be discarded and $J(\mathbf{x})$ set to 0.

1) Li's method: The simple formula has been proposed by Li et al. [13]:

$$J_{[\mathrm{Li}]}(\mathbf{x}) = \frac{|\lambda_2|}{|\lambda_3|}\left(|\lambda_2| - |\lambda_1|\right) \qquad (6)$$

2) Frangi's method: more advanced filtering has been proposed by Frangi et al. [12]. He introduces three quantities for different properties: $\mathcal{R}_\mathcal{B}$ for quantification of the relative amplitude of $|\lambda_1|$, $\mathcal{R}_\mathcal{A}$ for discrimination of tubular structures from planar structures, and S for quantification of the strength of all second order features:

$$\mathcal{R}_\mathcal{B} = \frac{|\lambda_1|}{\sqrt{|\lambda_2\lambda_3|}}, \quad \mathcal{R}_\mathcal{A} = \frac{|\lambda_2|}{|\lambda_3|}, \qquad (7)$$

$$\mathcal{S} = \| \mathcal{H} \|_F = \sqrt{\sum_{j=1,2,3} \lambda_j^2}. \qquad (8)$$

The two quantities $\mathcal{R}_\mathcal{A}$, $\mathcal{S}$ should be maximized ($\mathcal{R}_\mathcal{A}$ up to 1) and $\mathcal{R}_\mathcal{B}$ should be low or close to 0. They are combined into a single tubularness measure [12]:

$$J_{[\mathrm{Fra}]}(\mathbf{x}) = \left(1 - e^{-\frac{\mathcal{R}_\mathcal{A}^2}{2\alpha^2}}\right)\left(e^{-\frac{\mathcal{R}_\mathcal{B}^2}{2\beta^2}}\right)\left(1 - e^{-\frac{\mathcal{S}^2}{2c^2}}\right) \qquad (9)$$

Frangi et al. [12] recommends to set to $\alpha = \beta = 0.5$ and the parameter c is set experimentally.

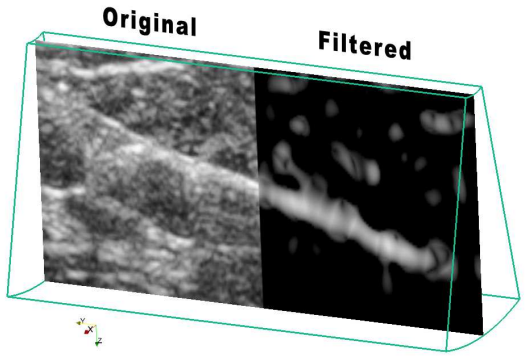

Fig. 1. 3D volume of breast biopsy with needle. The left part of the slice contains the original data and the right part contains the data filtered by method of Frangi [12].

B. Tool localization

The input of a tool localization algorithm consists of multiple attributes for each voxel $\mathbf{x}$: intensity $I(\mathbf{x})$, tubularness measure $J(\mathbf{x})$ and local principal orientation $\mathbf{k}(\mathbf{x})$.

We use the model fitting method based on RANSAC [9] for robust estimation of the tool location. This method works in several steps:

1. Pre-segmentation – the set of all voxels $\mathcal{X}$ is reduced to the group of tentative tool candidates $\mathcal{X}_t$. A novel pre-segmentation, which uses two attributes $I(\mathbf{x}), J(\mathbf{x})$ is proposed in Section II-B.
2. Axis localization – an approximate position of the tool axis is estimated by a randomized procedure RANSAC. It also produces a set of consistent points $\mathcal{X}_{\mathrm{inl}} \subseteq \mathcal{X}_t$, also known as *inliers* (Section II-C).
3. Local optimization – a more accurate solution is found using local optimization of curve parameters on the set of inliers $\mathcal{X}_{\mathrm{inl}}$.
4. Tip localization – the endpoint of the tool is identified as a significant drop in the intensity along the axis by the method of Barva [4].

The axis is represented by a spatial parametric polynomial curve $a(t; \mathbf{R}) : \mathbb{R} \to \mathbb{R}^3$ of order $n-1$ [9]:

$$a(t; \mathbf{R}) = \underbrace{\begin{pmatrix} r_{11} & \cdots & r_{1n} \\ r_{21} & \cdots & r_{2n} \\ r_{31} & \cdots & r_{3n} \end{pmatrix}}_{\mathbf{R}} \begin{pmatrix} 1 \\ t \\ \vdots \\ t^{n-1} \end{pmatrix}; \quad t \in \mathbb{R} \qquad (10)$$

$n = 2$ is used for thick electrodes which are expected to remain straight and $n = 3$ otherwise. The curve paremeters $\mathbf{R}$ can be determined by n control points $\mathbf{p}_i \in \mathbb{R}^3$, $i = 1 \ldots n$ through which it is required to pass [9].

Pre-segmentation: The tentative tool voxels $\mathcal{X}_\mathrm{t} \subseteq \mathcal{X}$ are selected according to the attributes $\mathbf{m}_1(\mathbf{x}) = [I(\mathbf{x})\ J(\mathbf{x})]$ pre-computed by line filtering (Section II-A). The decision function is defined as a linear classifier [6] using the attributes $\mathbf{m}_1(\mathbf{x})$:

$$\mathcal{X}_t = \{\mathbf{x} \in \mathcal{X} \mid (\mathbf{w} \cdot \mathbf{m}_1(\mathbf{x}) \geq w_0\}, \qquad (11)$$

where $\mathbf{w}$ is weight vector and w_0 is a bias. The parameters $\mathbf{w}$ and w_0 are learned from the training data with ground truth as the Fisher's linear discriminant (FLD) [6] which finds the best separating hyperplane. Pre-segmentation using two attributes gives better results (in terms of ratio of true positives and true negatives) than doing simple thresholding like in [9] (Section III-B). It is possible to use other classifiers, e.g. SVM or AdaBoost [6].

C. Tool model

We propose a new model of the tool appearance in 3D US images using the pre-processed volume data (Section II-A). The model is used by the tool localization algorithm (Section II-B). It consists of a function $q(\mathbf{x}, \mathbf{R})$ classifying voxel $\mathbf{x}$ as either a tool ($q = 1$) or a background ($q = 0$); and a cost function $C(\mathcal{X}_{\text{inl}}; \mathbf{R})$ quantifying how well the model parameters $\mathbf{R}$ fit the set of observations $\mathcal{X}_{\text{inl}}$ consistent with the model. The tool shape, i.e. curve parameters $\mathbf{R}$, are first estimated roughly by maximizing the number of tool voxels (inliers set $\mathcal{X}_{\text{inl}}$) as determined by q via RANSAC, and then refined by minimization of the cost function $C(\mathcal{X}_{\text{inl}}, \mathbf{R})$ [9].

The model (both functions $q(\mathbf{x}, \mathbf{R})$ and $C(\mathcal{X}_{\text{inl}}, \mathbf{R})$) needs to compute for each voxel $\mathbf{x}$ the distance to the curve $a(t, \mathbf{R})$. We compute the approximative distance

$$d(\mathbf{x}; \mathbf{R}) = \|\mathbf{x} - a(t_0; \mathbf{R})\|, \tag{12}$$

where the parameter t_0 is chosen to minimize the distance by a fast approximative procedure based on projecting x onto a straight line [9]. Then, we compute the normalized local derivative of $a(t_0, \mathbf{R})$.

$$\mathbf{a}_t(\mathbf{x}, \mathbf{R}) = c_t \frac{\partial a(t, \mathbf{R})(t_0)}{\partial t}, \tag{13}$$

where c_t is a normalization constant such that $\|\mathbf{a}_t(\mathbf{x}, \mathbf{R})\| = 1$. Finally, the dot product is computed to measure the consistency of $\mathbf{k}(\mathbf{x}, \mathbf{R})$ and $\mathbf{a}_t(\mathbf{x}, \mathbf{R})$:

$$b(\mathbf{x}; \mathbf{R}) = |\mathbf{k}(\mathbf{x}) \cdot \mathbf{a}_t(\mathbf{x}, \mathbf{R})| \,. \tag{14}$$

1) Classification function $q(\mathbf{x}, \mathbf{R})$: The classification function $q(\mathbf{x}, \mathbf{R})$ uses four attributes for each voxel $\mathbf{x} \in \mathcal{X}_t$:

$$\mathbf{m}_2(\mathbf{x}) = [I(\mathbf{x})\ J(\mathbf{x})\ d(\mathbf{x}, \mathbf{R})\ b(\mathbf{x}, \mathbf{R})] \tag{15}$$

and it is defined as a linear classifier [6]

$$q(\mathbf{x}, \mathbf{R}) = \begin{cases} 1, & \text{if } (\mathbf{w} \cdot \mathbf{m}_2(\mathbf{x}) \geq w_0)\,, \\ 0, & \text{if } (\mathbf{w} \cdot \mathbf{m}_2(\mathbf{x}) < w_0)\,, \end{cases} \tag{16}$$

where $\mathbf{w} = [w_1\, w_2\, w_3\, w_4]$ is a weight vector and w_0 is a bias. These parameters are learned from the training data with ground truth as the FLD [6].

2) Cost function $C(\mathcal{X}_{\text{inl}}, \mathbf{R})$: The model cost function $C(\mathcal{X}_{\text{inl}}, \mathbf{R})$ is defined using the discriminant function of the linear classifier from the previous definition (16)

$$C(\mathcal{X}_{\text{inl}}, \mathbf{R}) = \sum_{\mathbf{x} \in \mathcal{X}_{\text{inl}}} (\mathbf{w} \cdot \mathbf{m}_2(\mathbf{x}) - w_0)\,. \tag{17}$$

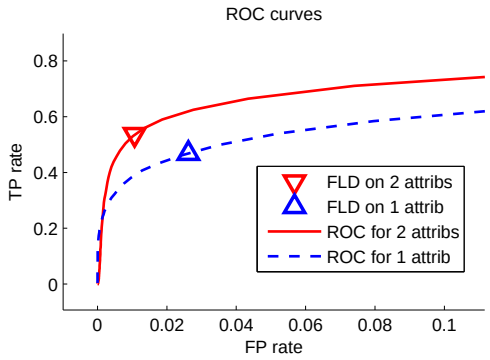

Fig. 2. ROC curves for pre-segmentation classifier trained on: a) two attributes $I(\mathbf{x})$ and $J(\mathbf{x})$, b) single attribute $I(\mathbf{x})$. The classifier found by FLD (Section II-B) is shown by color mark $\triangledown$.

III. Results

Experiments have been done on a PVA cryogel phantom [14] with electrode of diameter 0.3 mm. Eight 3D ultrasound images of size $53 \times 71 \times 260$ voxels have been acquired using the probe with central frequency 7.5 MHz from different positions.

The proposed method and other localization methods were implemented in MATLAB[1] and tested on a PC with Intel Core 4 processor at 2.83 GHz. The Hessian matrices were computed using a code by Almar Klein [2].

A. Tool enhancement evaluation

The contrast enhancement of tool voxels $\mathcal{X}_{tool}$ compared to background voxels $\mathcal{X}_{bg}$ (both sets are ground-truth) was evaluated using Weber contrast as:

$$W(I) = \frac{\overline{I(\mathcal{X}_{tool})} - \overline{I(\mathcal{X}_{bg})}}{\overline{I(\mathcal{X}_{bg})}}, \tag{18}$$

where $\overline{I}$ denotes the mean. The same Weber contrast can be computed on enhanced image $W(J)$.

The mean factor of improvement $W(J)/W(I)$ was $2.3\times$ by the method of Li and $4.2\times$ by the method of Frangi. The processing time was $8 - 10$ seconds for the whole volume.

B. ROC curve analysis of the pre-segmentation

We evaluated the quality of the pre-segmentation (Section II-B) using reciever operating characteristics (ROC) curve [6]. We want to reduce number of FPs in pre-segmentation, therefore we plot ROC curve (Fig. 2) only for FP rate less than 10%. We observed that pre-segmentation using two attributes, the number of TPs is increased by 25% for the 4% FP rate, and the number of TPs is increased by 40% for 1% FP rate than using only a single intensity attribute.

[1]The MathWorks, Natick, MA
[2]http://www.mathworks.com/matlabcentral/fileexchange/19696

Localization Algorithm	Axis acc. [mm]	Fails [%]	Time [sec]
RANSAC+AxShp	0.42 ± 0.22	61%	1.90
RANSAC+IntDstr	0.44 ± 0.18	53%	3.86
RANSAC+LineFilter	0.78 ± 0.35	15%	5.33

TABLE I
AXIS ACCURACY, PERCENTAGE OF FAILURES AND TIME WITHOUT PRE-PROCESSING FOR DIFFERENT LOCALIZATION ALGORITHMS.

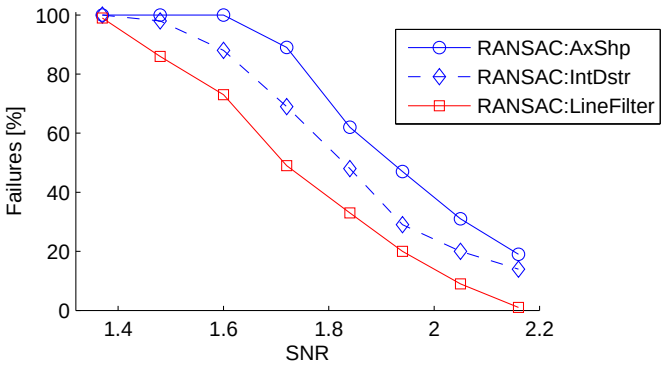

Fig. 3. The illustration of robustness evaluation of localization algorithms for varying SNR: measured number of failures (in percent).

C. Tool localization evaluation

The axis accuracy ϵ_{axis} measures the deviation from true axis location in mm [9]. The result is considered a failure when $\epsilon_{axis} > 3$ mm. The failures are reported separately.

The proposed method is compared to other localization methods based on model fitting using RANSAC with models AxShp and $\mathrm{IntDstr}$ [9]. Table I shows that the proposed model has the least failures on real data of PVA phantom. The line filtering was useful in this case for filtering-out 2D structures.

We also evaluate the robustness (number of failures) of localization on simulated data (mimicking the needle in breast tissue) with varying intensity of the tool with respect to the background. The signal to noise ratio (SNR) quantifies the quality of data $\mathrm{SNR} = \overline{I}(\mathcal{X}_{tool})/\overline{I}(\mathcal{X}_{bg})$. For each SNR level, the datasets were split into 19 testing and 9 training datasets. The model fitting algorithm was run 15 times with different random seed on each dataset. The comparison of robustness (Fig. 3) show that the proposed model with line filtering is the most robust among the tested group.

IV. CONCLUSIONS

We proposed method for tool localization in US which exploits its 1D shape. The tool contrast can be enhanced by line filtering methods based on eigen-analysis of the Hessian matrix for each voxel. The model fitting localization algorithm was improved using line filtered data and the number of failures has been reduced at the expense of additional pre-processing time. Note that no manual selection of region of interrest (ROI) was done. The local optimization using 4 attributes does not give as accurate results as previous models which needs to be further investigated.

In the future work, the pre-processing time can be significantly reduced by employing a cascade classifier, doing filtering only on voxels which will have passed an initial thresholding step. It would be also interresting to combine intensity distribution model [9] with line filtering in order to obtain even more robust tool localization.

ACKNOWLEDGMENTS

A dataset of breast biopsy is a courtesy of GE Medical Systems. The author Marián Uherčík was supported by an EC project MEST-CT-2005-021024 WARTHE. The author Jan Kybic was supported by Czech Ministry of Education project 1M0567.

REFERENCES

[1] A. Abati and A. Simsir, "Breast fine needle aspiration biopsy: prevailing recommendations and contemporary practices," *Clinics in laboratory medicine*, vol. 25, no. 4, pp. 631–654, December 2005.
[2] R. L. Alterman, D. Sterio, A. Beric, and P. J. Kelly, "Microelectrode recording during posteroventral pallidotomy," *Neurosurgery*, vol. 44, no. 2, pp. 315–321, February 1999.
[3] T. Peters, "Image-guidance for surgical procedures," *Physics in Medicine and Biology*, vol. 51, no. 14, pp. R505–R540, 2006.
[4] M. Barva, M. Uherčík, J.-M. Mari, J. Kybic, J.-R. Duhamel, H. Liebgott, V. Hlaváč, and C. Cachard, "Parallel integral projection transform for straight electrode localization in 3-D ultrasound images," *IEEE Trans. on UFFC*, vol. 55, no. 7, pp. 1559–1569, July 2008.
[5] M. Uherčík, J. Kybic, H. Liebgott, and C. Cachard, "Multi-resolution parallel integral projection for fast localization of a straight electrode in 3D ultrasound images," in *ISBI*, May 2008, pp. 33–36.
[6] R. O. Duda, P. E. Hart, and D. G. Stork, *Pattern Classification (2nd Edition)*. Wiley-Interscience, November 2000.
[7] H. Zhou, W. Qiu, M. Ding, and S. Zhang, "Automatic needle segmentation in 3D ultrasound images using 3D improved Hough transform," in *Proceedings of SPIE Medical Imaging*, 2008.
[8] W. Qiu, M. Ding, and M. Yuchi, "Needle segmentation using 3D quick randomized Hough transform," in *Proceedings of SPIE Medical Imaging*, 2008, pp. 449–452.
[9] M. Uherčík, J. Kybic, H. Liebgott, and C. Cachard, "Model fitting using RANSAC for surgical tool localization in 3D ultrasound images," CMP, K13133 FEE Czech Techn. Univ., Prague, Research Report CTU–CMP–2009–11, September 2009.
[10] M. A. Fischler and R. C. Bolles, "Random sample consensus: A paradigm for model fitting with applications to image analysis and automated cartography," *CACM*, vol. 24, no. 6, pp. 381–395, June 1981.
[11] M. Orkisz, L. Valencia, and M. Hoyos, "Models, algorithms and applications in vascular image segmentation," *MG&V*, vol. 17, no. 1, pp. 5–33, 2008.
[12] A. Frangi, W. Niessen, K. Vincken, and M. Viergever, "Multiscale vessel enhancement filtering," in *In proceedings of MICCAI*. Springer Berlin / Heidelberg, 1998, pp. 130+.
[13] Q. Li, S. Sone, and K. Doi, "Selective enhancement filters for nodules, vessels, and airway walls in two- and three-dimensional CT scans," *Medical Physics*, vol. 30, no. 8, pp. 2040–2051, 2003.
[14] J. Fromageau, E. Brusseau, D. Vray, G. Gimenez, and P. Delachartre, "Characterization of PVA cryogel for intravascular ultrasound elasticity imaging," *IEEE Trans. on UFFC*, vol. 50, no. 10, pp. 1318–1324, Oct. 2003.